

Dark matter physics, flavor physics and LHC constraints in the dark matter model with a bottom partner

Tomohiro Abe^{1,2}, Junichiro Kawamura³, Shohei Okawa⁴ and Yuji Omura²

¹ *Institute for Advanced Research, Nagoya University, Nagoya 464-8602, Japan*

² *Kobayashi-Maskawa Institute for the Origin of Particles and the Universe,
Nagoya University, Nagoya 464-8602, Japan*

³ *Department of Physics, Waseda University, Tokyo 169-8555, Japan*

⁴ *Department of Physics, Nagoya University, Nagoya 464-8602, Japan*

Abstract

In the scenario that a dark matter (DM) is a weakly interacting massive particle, there are many possibilities of the interactions with the Standard Model (SM) particles to achieve the relic density of DM. In this paper, we consider one simple DM model where the DM candidate is a complex scalar and interacts with the SM particles via exchange of the Higgs particle and an extra quark, named bottom partner. The extra quark carries the same quantum number as the right-handed down-type quarks and has Yukawa couplings with the DM candidate and the right-handed down-type quarks. The Yukawa interactions are not only relevant to the thermal relic density of the DM, but also contribute to the flavor physics, such as the $\Delta F = 2$ processes. In addition, the flavor alignment of the Yukawa couplings is related to the decay modes of the extra quark. Then, we can find the explicit correlations among the physical observables in DM physics, flavor physics and the signals at the LHC. Based on the numerical analyses of the thermal relic density, the direct detection of the DM and the current LHC bounds using the latest results, we survey our predictions for the $\Delta F = 2$ processes. We investigate the perturbative bound on the Yukawa coupling, as well. Study of a fermionic DM model with extra scalar quarks is also given for comparison.

1 Introduction

The cosmological observations exhibit the existence of the dark sector in our universe. Especially, the existence of a dark matter (DM) is supported by the many independent observations and driving particle physicists to build the Beyond Standard Models (BSMs). Surprisingly, the WMAP and the Planck experiments have made it known that the relic density of DM is about 5 times larger than the one of the baryon in our universe [1,2]. The Standard Model (SM) succeeds in describing almost all experimental results in particle physics, but such a large DM density definitely suggests unknown physics beyond the SM, which resides out of the region that the current experiments have already reached.

Motivated by introducing DMs, a lot of ideas have been proposed so far. One simple popular idea is as follows. DM candidates are neutral under the electromagnetic and $SU(3)_c$ symmetries, and interact with the SM particles via the electroweak gauge couplings. In this case, the DM is originated from the fields charged under the $SU(2)_L \times U(1)_Y$ gauge symmetry and the DM mass region is explicitly revealed by taking the relic density of DM into account.*

There are other possibilities that DM candidates do not dominantly interact with the SM particles via the electroweak gauge couplings. In this kind of model, DMs may couple with the SM Higgs. In addition, DMs may have Yukawa couplings with SM particles. If they are complex scalars which are neutral under the SM gauge groups, such a Yukawa coupling is possible introducing extra quarks or leptons. Such a simple extended SM has been well studied so far, and it would be one of the best candidates for the BSM, because they do not drastically change the SM predictions [4–10]. Besides, it is also very interesting and attractive that such a simple model can be tested by many observations in not only dark matter physics and the LHC experiments, but also flavor physics.† The Yukawa couplings between the DMs and the SM particles are generally flavor-dependent, so that the contributions to flavor changing processes modify the SM predictions. If DMs are discovered in the LHC and DM experiments in future, we have to test a lot of DM models in many observables. In this simple model, we could find some correlations and give some explicit predictions to the results in future experiments.

In this letter, we concentrate on a DM model with a scalar DM candidate (X) and a vector-like quark (F) whose SM charges are the same as the ones of the right-handed down-type quarks. X is a complex scalar and neutral under the SM gauge groups. It couples with right-handed down-type quarks (d_R^i) via the Yukawa couplings involving F : $\lambda_i \bar{F}_L X^\dagger d_R^i$ ($i = d, s, b$). Besides, X interacts with the SM Higgs doublet, denoted by H , via a 4-point coupling (i.e. $\lambda_H |X|^2 |H|^2$). Then, the annihilation processes of the DM are given by the F and H exchanging diagrams. Note that this setup differs from the models in Refs. [4–8,10] and the integrated quantitative study including flavor physics, which has not been done in Refs. [4–10], is given in this paper.

As we see in Sec. 3.2, the contribution of the F exchanging diagrams cannot be enough large to achieve the relic abundance of the DM thermally without large Yukawa couplings.

* See, for instance, Ref. [3].

† The correlations have been discussed in the models with flavor symmetry [11–13].

This is because the s -wave contribution is suppressed by the down-type quark masses. Then, λ_i should be large as far as λ_H is small. Besides, the relation, $\lambda_b \gg \lambda_{d,s}$, should be satisfied to evade the strong bounds from the flavor physics and the LHC experiments as well as the direct detection of the DM. This relation for λ_i leads that F dominantly decays to the bottom quark and X , according to the sizable λ_b . (In this sense, we call F a "bottom partner.") Eventually, we can approximately discuss the DM physics and LHC physics using only three parameters: masses of F and X , and λ_b .

In our model, we do not assign any flavor symmetry, so that λ_d and λ_s cannot be vanishing, even though $\lambda_b \gg \lambda_{d,s}$ is assumed. In general, Flavor physics is very sensitive to the contributions of new physics, even if the new physics scale is above TeV-scale. Then, tiny λ_d and λ_s are expected to contribute to the flavor physics measured by the (future) flavor experiments, and we can expect that our results of the DM physics can be indirectly tested by the observables in flavor physics. In fact, we discuss our predictions of the $\Delta F = 2$ processes, based on our results in the dark matter and LHC physics, in Sec. 3.3. We find some correlations and give some explicit predictions in the flavor physics. We can expect that our DM is discovered in the LHC and DM experiments. Then, we suggest that our simple model can be tested by the precise measurements of the $\Delta F = 2$ processes. This is our motivation of our work. In Sec. 4, we also compare our results with the ones in another setup, where there are a fermionic DM (\tilde{X}) and an extra scalar quark (\tilde{F}) instead of X and F . \tilde{X} is a Dirac fermion in our study.

In Sec. 2, we introduce the setup of our model. Then, we study our signals at the LHC, dark matter physics and flavor physics in our model, in Secs. 3.1, 3.2 and 3.3 respectively. In Sec. 3.2.3, the triviality bound on the Yukawa couplings is studied. In Sec. 4, we discuss another setup that a fermionic DM (\tilde{X}) and an extra scalar quark (\tilde{F}) are introduced instead of X and F , and compare our predictions in both cases. Sec. 5 is devoted to the summary.

2 Setup

In this section, we introduce our model with a vector-like quark. Similar setup has been proposed, motivated by the DM physics and the LHC physics [4–10].

We introduce an extra down-type quark, F , carrying SM charges as in Table 2. F

Fields	spin	SU(3) _c	SU(2) _L	U(1) _Y	U(1) _X
F	1/2	3	1	$-1/3$	1
X	0	1	1	0	-1

Table 1: Extra fields in our model with global U(1)_X.

is a dirac fermion and the charge assignment is the same as the one of the right-handed down-type quarks, d_R^i ($i = 1, 2, 3$). In our notation, (d^1, d^2, d^3) correspond to (d, s, b) .

We assign global $U(1)_X$ charges to F to distinguish with the SM down-type quarks. In addition, we introduce a complex scalar, denoted by X . X is also charged under the global $U(1)_X$ symmetry, and it becomes stable. The charge assignment is summarized in Table 2. Now we can write down the potential for the extra quark and the scalar:

$$V = V_F + V_X, \quad (1)$$

$$V_F = m_F \overline{F}_L F_R + \lambda_i \overline{F}_L X^\dagger d_R^i + h.c., \quad (2)$$

$$V_X = m_X^2 |X|^2 + \lambda_H |X|^2 |H|^2 + \lambda_X |X|^4 - m_H^2 |H|^2 + \lambda |H|^4. \quad (3)$$

The each coupling, λ_i , is the Yukawa coupling to induce the decay of F : $F \rightarrow X d^i$. Note that V_X is the potential for the scalars including the SM Higgs (H). λ_H plays a crucial role in dark matter physics, as discussed in Sec. 3.2.

3 Phenomenology

In our model, there are several parameters that can be determined combining the analyses of dark matter physics, flavor physics and the direct searches at the LHC. The relevant parameters in our study are as follows:

$$m_X, m_F, \lambda_H, \lambda_b, Re(\lambda_s), Im(\lambda_s), Re(\lambda_d), Im(\lambda_d). \quad (4)$$

Note that we can define λ_b as a real one, without loss of generality. In order to avoid the stringent bounds from flavor physics and direct detections of the DM, we assume the following relation,

$$|\lambda_b| \gg |\lambda_d|, |\lambda_s|. \quad (5)$$

In this case, F mainly decays to X and the bottom quark, and the dominant annihilation process of X is $X X^\dagger \rightarrow \bar{b} b$ in the t -channel, as far as λ_H is relatively small. This means that λ_b , as well as m_X and m_F , can be fixed by the direct search for F and X in the $b\bar{b}$ signal accompanied by the large missing energy at the LHC and the DM observables, i.e., the relic abundance and the direct/indirect detections.

On the other hand, λ_d and λ_s are tiny in our setup, but not vanishing in general. The Yukawa couplings are strongly constrained by flavor physics and should be less than $\mathcal{O}(0.01)$, as we see in Sec. 3.3. In other words, we can expect the sizable deviations in physical observables in flavor violating processes. In fact, we will find some correlations among the observables in the $\Delta F = 2$ processes and derive explicit predictions for them, taking the analyses of the DM and LHC physics into account, in Sec. 3.3.

3.1 Constraints from the direct searches at the LHC

First, let us discuss the collider bounds from the new physics searches. In our model, the extra quark (F), which we call a *bottom partner*, is produced at the LHC and mainly decays into a bottom quark and a DM, via the Yukawa coupling, λ_b . This signal is similar to the one in supersymmetric models: that is, $b\bar{b} + E_T^{\text{miss}}$. In order to extract the exclusion

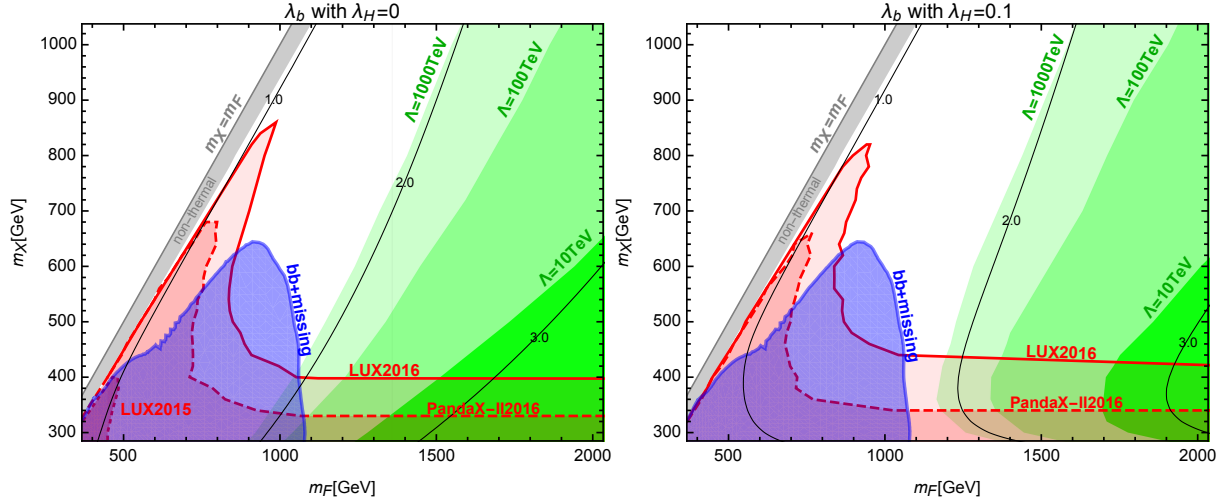


Figure 1: The required values of λ_b for $\Omega h^2 = 0.1198 \pm 0.0015$. The blue regions are excluded by the bb +missing at the LHC. The red regions are excluded by the direct detection experiments. The Yukawa couplings diverge below 1000 TeV in the green regions.

limit for the bottom partner, we generate the UFO model file [14] using FeynRules [15]. We use the MadGraph5 [16] to simulate signal events with a pair produced vector-like quarks at the leading order (LO) with up to an parton. The generated events are passed into PYTHIA6 [17] and DELPHES3 [18] to accommodate parton showering and fast detector simulation. The matrix element is matched to parton showers according to the MLM scheme [19]. The generated hadrons are clustered using the anti- k_T algorithm [20] with the radius parameter $\Delta R = 0.4$. In the analysis for the $bb + E_T^{\text{miss}}$ search, we assume that the b-tagging efficiency obeys a formula $0.80 \times \tanh(0.003p_T) \times 30/(1 + 0.086p_T)$ which is employed in the ATLAS DELPHES card in the MadGraph5, then we rescale the event weight by multiplying a factor of 1.2 to emulate the experimental b-tagging efficiency where the working point is 77% for $t\bar{t}$ events.

Following the analysis of $bb + E_T^{\text{miss}}$ in Ref. [21], we draw the exclusion limit in Fig. 1. This result is given referring the latest data of the LHC Run-II with $\sqrt{s} = 13$ TeV and 3.2 fb^{-1} . We compared the expected number of events in each signal region defined in the ATLAS analysis with their 95% C.L exclusion limits shown in the ref. [21]. The Yukawa couplings λ_i potentially induce large production cross section of the extra-quark pairs by the t-channel process mediated by X , but this process is suppressed by the parton distribution function in our case, $\lambda_b \gg \lambda_{s,d}$.

3.2 Dark Matter Physics

Next, we survey the relic abundance and the direct/indirect detection of X .

3.2.1 Relic DM abundance

Annihilation and coannihilation of X and X^\dagger to the SM particles should be sufficiently large in order to be consistent with the cosmological observation of the DM abundance in our universe. Those processes are governed by the F exchanging in t -channel and the Higgs exchanging in s -channel. Depending on the size of λ_H , the t -channel is dominant in the DM annihilation. We employ `micrOMEGAs_3.6.9.2` [22] to evaluate the relic abundance of the DM. In our numerical analysis, we use the value proposed by the Planck collaboration: $\Omega h^2 = 0.1198 \pm 0.0015$ [2].

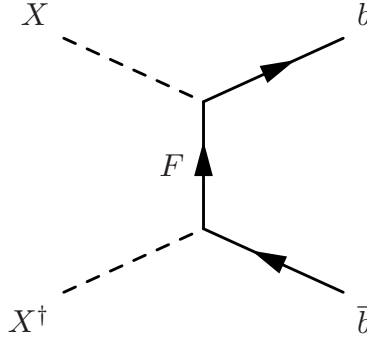


Figure 2: The dominant process of DM annihilation in the t -channel.

The main process of the DM annihilation is $X X^\dagger \rightarrow b \bar{b}$ given by λ_b in the t -channel shown in Fig. 2. The Yukawa coupling, $\lambda_b \bar{F}_L X^\dagger b_R$, depends on the chiralities of F and b , so that the bottom quark in the final state of the annihilation is right-handed in the massless limit of the quark. Then, we conclude that the s -wave contribution of the annihilation is strongly suppressed by the bottom quark mass, so that λ_b is required to be $\mathcal{O}(1)$ as far as λ_H is small and coannihilation is inefficient.

The coannihilation processes, such as $F \bar{F} \rightarrow g g$, may drastically decrease the relic density if m_F is close to m_X . In fact, the coannihilation contribution leads too small relic density of X in the region with $m_F \approx m_X$. The gray region in Fig. 1 corresponds to the one that predicts $\Omega h^2 < 0.1183$ that is out of the 1σ region of the Planck result. Our analysis for the DM density includes $X X^\dagger \rightarrow b \bar{b} g$ in addition to the annihilation and the coannihilation. This process has non-negligible contribution for $r \equiv m_F/m_X \lesssim 2$ and dominates over the t -channel for $r \lesssim 1.12$. Our analysis only includes the s -wave contribution of this process.

We see the required values of λ_b on the plane of m_F and m_X , in Fig. 1. λ_H is fixed at $\lambda_H = 0$ (left panel) and $\lambda_H = 0.1$ (right panel), respectively. On the solid lines, λ_b is fixed at 1, 2, 3 from left to right respectively, and the relic density satisfies the observed value. In the compressed region below $m_F = 1$ TeV, the mass difference between m_X and m_F is about 50 GeV to satisfy the Planck data within 1σ . As mentioned above, we see that $\mathcal{O}(1)$ λ_b is required in the most of parameter region.

3.2.2 Direct/indirect detections of DM

DMs, which largely exists in our universe and interacts with the SM quarks, can be detected by the observation of the DM scattering with nuclei. Recently, we can successfully draw the stringent exclusion lines thanks to a lot of efforts of the LUX [24, 25] and Panda [26] collaborations.

In the setup, where $\lambda_b \gg |\lambda_d|, |\lambda_s|$ is assumed, the tree-level contribution of the t -channel interaction to the direct detection cross section is sufficiently small and the significant contribution arises from the one-loop diagrams shown in Fig. 3. Especially, we find that the main contribution is the photon exchanging, generating the coupling of DM to the nucleon charge. Note that there is a logarithmic enhancement, $\log(m_b^2/m_F^2)$, in $m_F \gg m_b$ region [11–13]. DM can also scatter off gluons in the nucleon via F and b box diagrams. The contribution of the gluon scattering is sub-dominant and less than 10% of the photon exchanging in our parameter space. Our analysis includes both the one-loop contributions. We describe the excluded regions as the red ones in Fig. 1, using the central limits proposed by the LUX [24, 25] and Panda experiments [26], respectively.

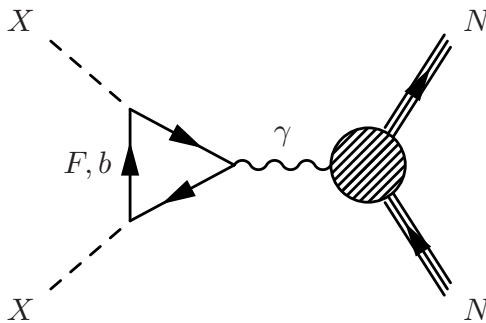


Figure 3: The dominant process in the cross section for the direct detection of X .

Let us comment on the bound from the DM experiments concerned with the indirect detections. X and X^\dagger existing in our universe annihilate into b and \bar{b} . The constraint on the cross section has been proposed by the Fermi-LAT collaboration [23]. Assuming that s -wave contribution is dominant in DM annihilations, the lower bound on the DM mass reaches about 200 GeV [23]. In our model, the annihilation is dominated by the p -wave contribution, which is much smaller at the present temperature than the one at the freeze-out temperature. Then, the bound from the indirect detection is not strict in our model, as far as λ_H is enough small for the t -channel in Fig. 2 to dominate over the Higgs exchanging. Note that one very strict exclusion limit on the annihilation cross section has been proposed recently in Refs. [27, 28], based on the latest result of the AMS-02 experiment [29]. If we consider the other setups, as discussed in Sec. 4, the upper bound on the annihilation cross section of DMs to $b\bar{b}$ is below the value required by the relic density. In terms of this, our setup suggests one way to achieve the correct relic density without any conflicts with the direct/indirect detections.

3.2.3 Triviality bound

In general, large Yukawa couplings bring cutoff scale to models because Yukawa couplings are asymptotic non-free. This cutoff scale is known as triviality bound. We calculate the triviality bound in this model because the large λ_b is required to reproduce the correct relic abundance of DM in our model as we can see from Fig. 1. The beta functions for λ_b and the QCD coupling are given as follows:

$$\beta_{\lambda_b} \simeq \frac{\lambda_b}{(4\pi)^2} \left(-8g_3^2 + 4\lambda_b^2 \right), \quad (6)$$

$$\beta_{g_3} \simeq \frac{1}{(4\pi)^2} \left(-\frac{19}{3}g_3^3 \right), \quad (7)$$

where g_3 is the QCD gauge coupling which is large and cannot be ignored. We estimate the triviality bound by solving the renormalization group equation with the beta functions at the one-loop level. We fill the regions where the triviality bound is below 1000 TeV with green color in Fig. 1.

3.3 Flavor Physics

Finally, we investigate our predictions in flavor physics, based on our results in Secs. 3.1 and 3.2. In our model, Flavor Changing Neutral Currents (FCNCs) are induced by the Yukawa couplings between quarks and the dark matter. λ^i are the extra flavor-dependent couplings and generate the FCNCs at the one-loop level. In the Yukawa couplings, the chiralities of the quarks are right-handed. Then, we find that the structure of chirality strongly suppresses the new physics contributions to the flavor violating processes.

3.3.1 $\Delta F = 2$ processes

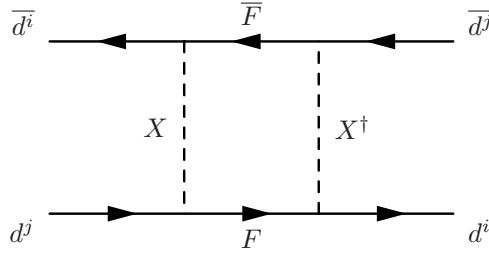


Figure 4: The box diagram to contribute to the $\Delta F = 2$ processes.

In the massless limit of the SM quarks, the box diagrams involving X and F , shown in Fig. 4, induce the operators relevant to the $\Delta F = 2$ processes:

$$\mathcal{H}_{eff}^{\Delta F=2} = (\tilde{C}_1)_{ij} (\bar{d}_R^i \gamma^\mu d_R^j) (\bar{d}_R^i \gamma^\mu d_R^j) + h.c.. \quad (8)$$

$\alpha_s(M_Z)$	0.1193(16) [31]	λ	0.22537(61) [31]
G_F	$1.1663787(6) \times 10^{-5} \text{ GeV}^{-2}$ [31]	A	$0.814^{+0.023}_{-0.024}$ [31]
m_b	$4.18 \pm 0.03 \text{ GeV}$ [31]	$\bar{\rho}$	0.117(21) [31]
m_t	$160^{+5}_{-4} \text{ GeV}$ [31]	$\bar{\eta}$	0.353(13) [31]
m_c	$1.275 \pm 0.025 \text{ GeV}$ [31]		
m_K	497.611(13) MeV [31]	m_{B_s}	5.3663(6) GeV [31]
F_K	156.1(11) MeV [32]	m_B	5.2795(3) GeV [31]
\hat{B}_K	0.764(10) [32]	F_{B_s}	$227.7 \pm 6.2 \text{ MeV}$ [32]
$(\Delta M_K)_{\text{exp}}$	$3.484(6) \times 10^{-12} \text{ MeV}$ [31]	F_B	$190.6 \pm 4.6 \text{ MeV}$ [32]
$ \epsilon_K $	$(2.228(11)) \times 10^{-3}$ [31]	\hat{B}_{B_s}	1.33(6) [32]
η_1	1.87(76) [33]	\hat{B}_B	1.26(11) [32]
η_2	0.5765(65) [34]	η_B	0.55 [34]
η_3	0.496(47) [35]		

Table 2: The input parameters relevant to our analyses. The CKM matrix, V_{CKM} , is written in terms of λ , A , $\bar{\rho}$ and $\bar{\eta}$ [31].

The Wilson coefficients at the one-loop level are given by,

$$(\tilde{C}_1)_{ij} = \frac{(\lambda_j \lambda_i^*)^2}{64\pi^2} \frac{1}{(m_F^2 - m_X^2)^2} \left\{ \frac{m_F^2 + m_X^2}{2} + \frac{m_X^2 m_F^2}{m_F^2 - m_X^2} \ln \left(\frac{m_X^2}{m_F^2} \right) \right\}. \quad (9)$$

The $K_0\text{-}\overline{K}_0$, $B_d\text{-}\overline{B}_d$, and $B_s\text{-}\overline{B}_s$ mixing are well investigated theoretically and experimentally. As shown in Fig. 1, λ_b is $\mathcal{O}(1)$. Then, $B_d\text{-}\overline{B}_d$ and $B_s\text{-}\overline{B}_s$ mixing become important even if $|\lambda_d|$ and $|\lambda_s|$ are small compared to λ_b . Besides, the physical observables associated with $K_0\text{-}\overline{K}_0$, in general, constrain new physics contributions, although their SM predictions still have large uncertainties (See e.g. [30]).

Here, we investigate our predictions in the following observables:

$$\Delta M_{B_d}, \Delta M_{B_s}, S_{\psi K}, S_{\psi\phi}, \epsilon_K. \quad (10)$$

We do not include ΔM_K , because of the large theoretical ambiguity. Among our parameters summarized in Eq. (4), we expect that m_F , m_X and λ_b are determined by the observables in the DM physics and the LHC experiments, as far as λ_H is small. Then, the other parameters, $Re(\lambda_s)$, $Im(\lambda_s)$, $Re(\lambda_d)$ and $Im(\lambda_d)$, are fixed by the observables in Eq. (10). We notice that the number of the parameters is smaller than the one of the observables, so that we can obtain an explicit prediction for the physical quantities measured by the flavor experiments.

In the $B_d\text{-}\overline{B}_d$ and $B_s\text{-}\overline{B}_s$ mixing, the representative observables relevant to the mixing are mass differences denoted by ΔM_{B_d} and ΔM_{B_s} . They are influenced by $(\tilde{C}_1)_{bd}$ and

$(\tilde{C}_1)_{bs}$ as follows:

$$\Delta M_{B_q} = 2 \left| M_{12}^{B_q} \right|^2 = 2 \left| (M_{12}^{B_q})_{\text{SM}} + \frac{1}{3} (\tilde{C}_1)_{bq} m_{B_q} F_{B_q}^2 \hat{B}_{B_q} \right|^2 \quad (q = d, s), \quad (11)$$

where $(M_{12}^{B_q})_{\text{SM}}$ is given by the top-loop contribution:

$$(M_{12}^{B_q})_{\text{SM}}^* = \frac{G_F^2}{12\pi^2} F_{B_q}^2 \hat{B}_{B_q} m_{B_q} M_W^2 \{ (V_{CKM})_{tb}^* (V_{CKM})_{tq} \}^2 \eta_B S_0(x_t). \quad (12)$$

$S_0(x)$ is defined in Appendix A.

The time-dependent CP violations, $S_{\psi K}$ and $S_{\psi\phi}$, are evaluated as follows including the new physics contributions:

$$S_{\psi K} = -\sin \varphi_{B_d}, \quad S_{\psi\phi} = \sin \varphi_{B_s}, \quad (13)$$

where φ_{B_q} is the phase of $M_{12}^{B_q}$: $M_{12}^{B_q} = |M_{12}^{B_q}| e^{i\varphi_{B_q}}$. The input parameters are summarized in Table 2, and the central values are used in our analyses.

In Fig. 5, we can see the deviations of ΔM_{B_d} and ΔM_{B_s} from the SM predictions, fixing $\lambda_{d,s}$ at $\lambda_d = 0.01$ (left panel) and $\lambda_s = 0.05$ (right panel). The solid lines predict 1 % and 5 % deviations respectively, compared to the SM predictions. The dotted lines correspond to the 2 %, 3 %, and 4 % deviations from bottom to top in each panel. As we see in those figures, the deviations are enough small to evade the bounds on the $\Delta F = 2$ processes, as far as $|\lambda_d| \leq 0.01$ and $|\lambda_s| \leq 0.05$ are satisfied. Note that there are still large uncertainties of the SM predictions for ΔM_{B_q} , and the CKMfitter collaboration suggests that 10 % deviations are still allowed according to the global analyses [30, 36]. If λ_d (λ_s) is set to 0.02 (0.1), the deviations become twice bigger than the values on Fig. 5. Then, we could conclude that the upper bounds on $|\lambda_d|$ and $|\lambda_s|$ are $\mathcal{O}(0.01)$ and $\mathcal{O}(0.05)$ respectively, in the region that the Landau poles do not appear below 1000 TeV.

In Fig. 6 and Fig. 7, we can see the bounds on the $\Delta F = 2$ processes, more clearly. We fix m_X , and m_F and λ_b , according to the requirement of the correct relic density within 1σ . The reference points we chose are $(m_X, m_F, \lambda_b) = (900 \text{ GeV}, 964.4 \text{ GeV}, 0.66)$ (Fig. 6) and $(m_X, m_F, \lambda_b) = (900 \text{ GeV}, 1795.7 \text{ GeV}, 2.32)$ (Fig. 7). On the blue bands, the deviations of $S_{\psi K}$ and $S_{\psi\phi}$ are within 1σ : $S_{\psi K} = 0.691 \pm 0.017$ and $S_{\psi\phi} = 0.015 \pm 0.035$ [31]. On the red (dashed) lines, the deviations of ΔM_{B_q} are 5 % (-5 %). The pink (dashed) lines predict 10 % (-10 %) deviations, respectively. In the red regions, the magnitudes of the deviations are less than 5 %. As we see in those figures, the regions for the $\Delta F = 2$ processes, where the magnitudes of the deviations are less than 5 %, correspond to $|\lambda_d| \lesssim 0.04$ (left panel) and $|\lambda_s| \lesssim 0.2$ (right panel) in Fig. 6. m_F and λ_b in Fig. 7 are bigger than in Fig. 6. Such a large m_F tends to suppress deviations of the observables, but large λ_b is required to achieve the correct relic density. Then, Fig. 7 shows that the allowed region becomes smaller in the heavy m_F case.

On the other hand, we can see the correlation between the flavor physics and the DM direct detection, especially in the left panel of Fig. 6. If $|\lambda_d|$ is large, the tree-level

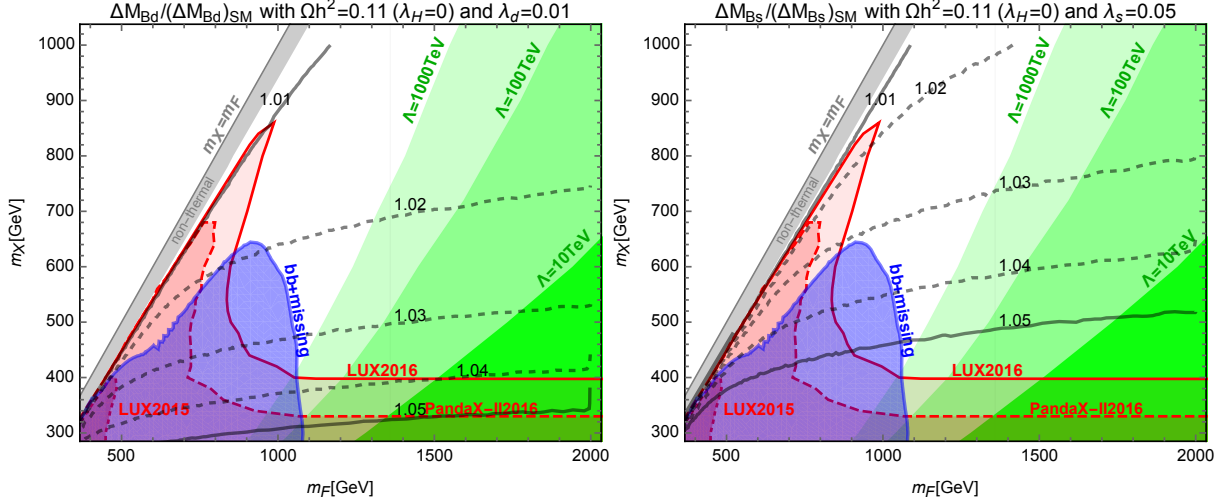


Figure 5: Predictions for the $\Delta F = 2$ processes. $\Omega h^2 = 0.1198 \pm 0.0015$ is satisfied. The blue region is excluded by the bb +missing at the LHC.

diagram, $X^\dagger d \rightarrow X^\dagger d$, sufficiently becomes large. The gray circle depicts the exclusion line of the LUX experiment [25], which was discussed in Sec. 3.2.2. The outside of the circle exceeds the upper bound on the cross section of the DM direct detection. Then, we see that the allowed region roughly corresponds to $|\lambda_d| \lesssim 0.04$. In the right panel of Fig. 6 and Fig. 7, the exclusion line is out of the figure. Note that the upper bound from the direct detection is roughly $|\lambda_d| \lesssim 0.15$, in the right panel of Fig. 7.

The observables of the K_0 - \bar{K}_0 mixing can be estimated as follows in our model. Their SM predictions are described by $(M_{12}^K)_{\text{SM}}$,

$$(M_{12}^K)_{\text{SM}}^* = \frac{G_F^2}{12\pi^2} F_K^2 \hat{B}_K m_K M_W^2 \{ V_c^2 \eta_1 S_0(x_c) + V_t^2 \eta_2 S_0(x_t) + 2V_c V_t \eta_3 S(x_c, x_t) \}. \quad (14)$$

x_i and V_i denote m_i^2/M_W^2 and $(V_{CKM})_{is}^* (V_{CKM})_{id}$, respectively. $\eta_{1,2,3}$ correspond to the NLO and NNLO QCD corrections. The each function is defined in Appendix A and the used values are summarized in Table 2. The physical observables on the K_0 - \bar{K}_0 mixing are denoted by ϵ_K and ΔM_K , which are described as

$$\epsilon_K = \frac{\kappa_\epsilon e^{i\varphi_\epsilon}}{\sqrt{2}(\Delta M_K)_{\text{exp}}} \text{Im}(M_{12}^K), \quad \Delta M_K = 2\text{Re}(M_{12}^K). \quad (15)$$

κ_ϵ and φ_ϵ are given by the observations: $\kappa_\epsilon = 0.94 \pm 0.02$ and $\varphi_\epsilon = 0.2417 \times \pi$. M_{12}^K include the new physics contribution and decomposed as follows in our model:

$$M_{12}^K = (M_{12}^K)_{\text{SM}} + (\tilde{C}_1)_{sd} \times \frac{1}{3} m_K F_K^2 \hat{B}_K. \quad (16)$$

The running correction is included at the one-loop level in our analysis.

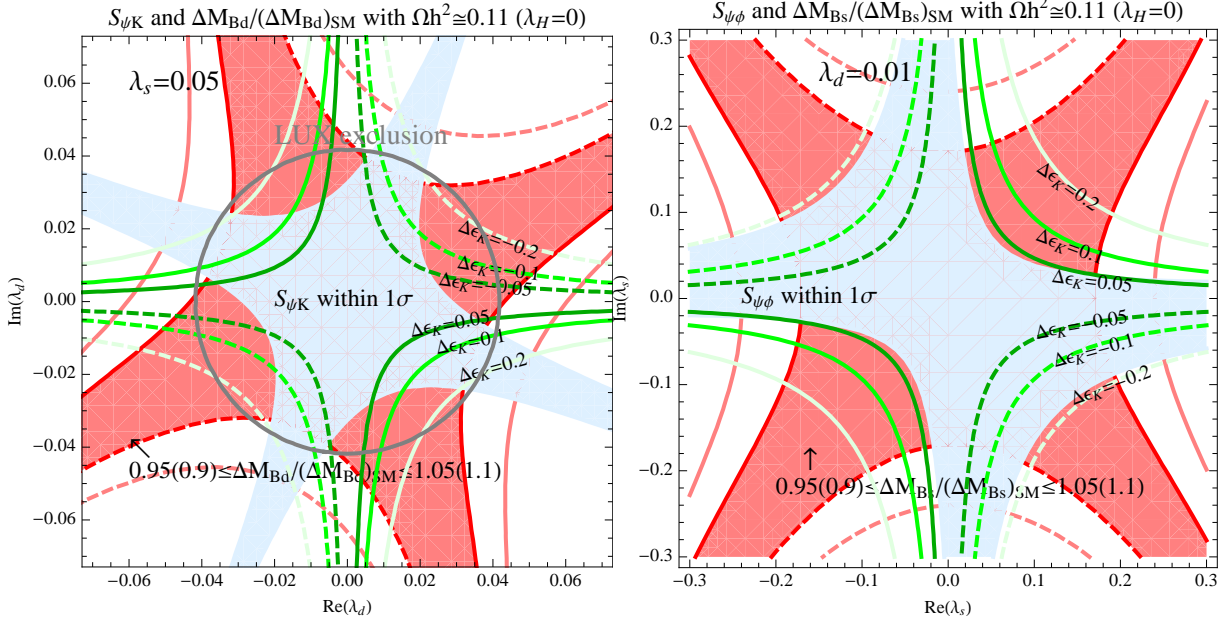


Figure 6: Predictions for the $\Delta F = 2$ processes. The other parameters are fixed by the relic abundance within 1σ : $(m_X, m_F, \lambda_b) = (900 \text{ GeV}, 964.4 \text{ GeV}, 0.66)$. The gray circle depicts the exclusion of the LUX experiment that is direct search of the DM [25]. The outside of the circle exceeds the upper bound on the cross section of the DM direct detection.

The predictions for the deviations of ϵ_K are depicted as green lines in Figs. 6 and 7. Once we assume that the deviations of the B_d - \bar{B}_d and B_s - \bar{B}_s mixing are discovered, we can principally predict the deviation of ϵ_K . The (dashed) dark, normal and light green lines depict the (-)5 %, (-)10 %, and (-)20 % deviations of ϵ_K respectively, compared to the SM prediction. On the each panel, $\lambda_s = 0.05$ (left) and $\lambda_d = 0.01$ (right) are assumed. In Fig. 6, they correspond to $(\Delta M_{B_s}/(\Delta M_{B_s})_{\text{SM}}, S_{\psi\phi}) = (1.004, 0.037)$ (left) and $(\Delta M_{B_d}/(\Delta M_{B_d})_{\text{SM}}, S_{\psi K}) = (1.003, 0.687)$ (right). In Fig. 7, the fixed λ_s and λ_d correspond to $(\Delta M_{B_s}/(\Delta M_{B_s})_{\text{SM}}, S_{\psi\phi}) = (1.025, 0.037)$ (left) and $(\Delta M_{B_d}/(\Delta M_{B_d})_{\text{SM}}, S_{\psi K}) = (1.015, 0.678)$ (right) respectively. Besides, the current limit on the direct detection of DM constrains the deviation of ϵ_K , depending on the mass region. As we see in the left panel of Fig. 6, $|\Delta\epsilon_K|$ cannot exceed about 0.2, in this compressed mass region.

3.3.2 $b \rightarrow s \gamma$ and the other observables

The $b \rightarrow s$ transitions may be good processes to test our models. The contributions of the new Yukawa couplings are, however, too small to find the deviations in flavor experiments. The structure of the chirality suppresses the photon- and Z -penguin diagrams. The chirality-flipped operators are suppressed by the quark masses on the external lines. One of the most important processes to test new physics is $b \rightarrow s \gamma$. The relevant operators,

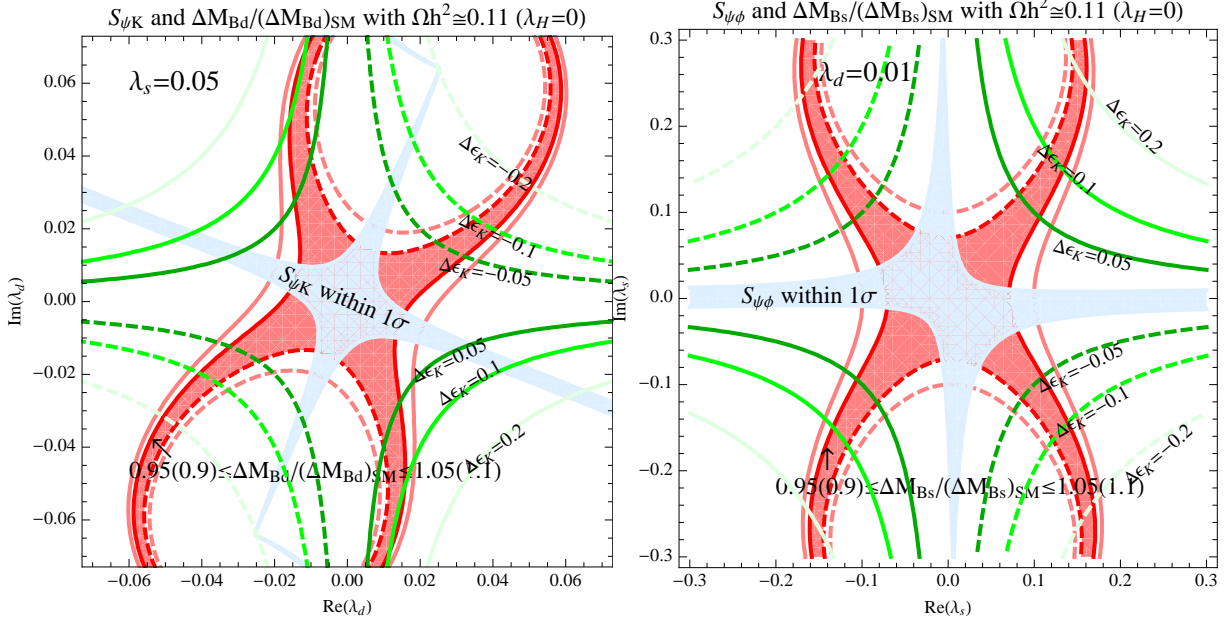


Figure 7: Predictions for the $\Delta F = 2$ processes. The other parameters are fixed by the relic abundance within 1σ : $(m_X, m_F, \lambda_b) = (900 \text{ GeV}, 1795.7 \text{ GeV}, 2.32)$. The exclusion lines proposed by the LUX experiment [25] are out of these parameter regions.

that contribute to the process, are

$$\mathcal{H}_{eff}^{b \rightarrow s \gamma} = C_7' (\bar{s}_L \sigma^{\mu\nu} b_R) F_{\mu\nu} + C_7' (\bar{s}_R \sigma^{\mu\nu} b_L) F_{\mu\nu}. \quad (17)$$

In our setup, the new contribution to C_7' is larger than the one to C_7 , because of the mass difference between m_b and m_s . The allowed new physics contribution is well summarized in Ref. [37]: $|C_7'| \lesssim 0.02$. Fixing λ_s at $\lambda_s = 0.1$, we estimate $|C_7'|$ as $|C_7'| \lesssim 0.004$, as far as the deviation of ΔM_{B_s} is less than 10 %. Then, we conclude that it is difficult to test our model, using the $b \rightarrow s \gamma$ process.

Some excesses have been reported in the $b \rightarrow s$ transition associated with two leptons in the final state. As pointed out in Ref. [38], the excess on the flavor universality of $B \rightarrow K l l$ favors $(\bar{s}_L \gamma^\mu b_L)(\bar{l} \Gamma^\mu l)$. Our model enhances $(\bar{s}_R \gamma^\mu b_R)(\bar{l} \Gamma^\mu l)$, so that it may be difficult to explain the anomaly.

4 Comparison with the Dirac DM case

It is important to see differences among the predictions of DM models with extra colored particles, as well. As discussed above, one of the stringent constraints is from the direct detection of the complex scalar DM. This is because the s -wave contribution of the annihilation cross section of DMs in the t -channel is suppressed by the fermion mass, and then $\mathcal{O}(1)$ Yukawa coupling, λ_b , is required to achieve the correct relic density. If we consider a

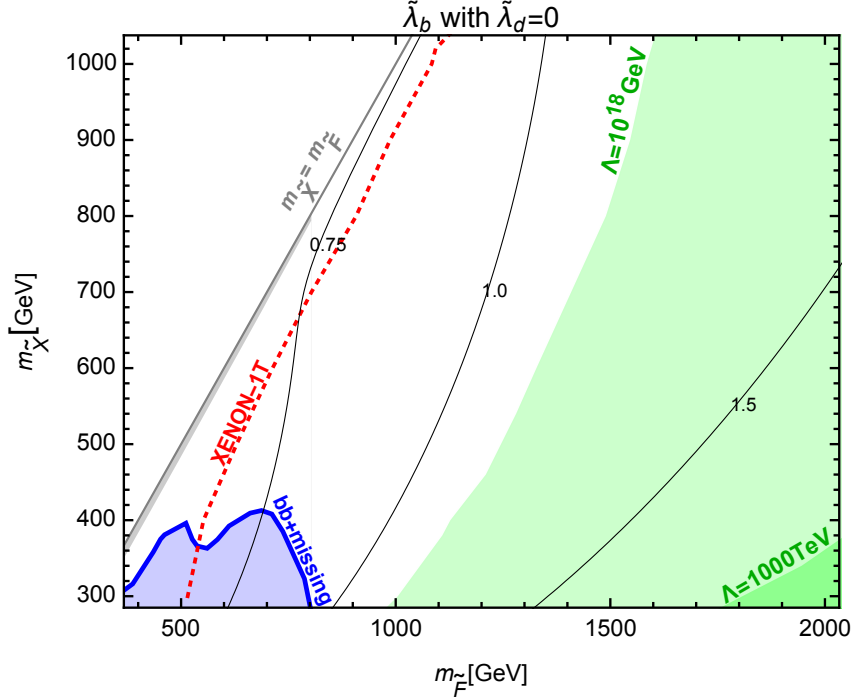


Figure 8: The required values of $\tilde{\lambda}_b$ for the correct relic abundance in the Dirac-fermion DM model with an extra colored scalar particle. The blue region is excluded by the bb +missing at the LHC.

Dirac-fermion DM (\tilde{X}) introducing an extra colored scalar field (\tilde{F}) instead of X and F , we can expect that the s -wave contribution is enhanced by the DM mass. The Yukawa couplings relevant to the annihilation are given by

$$\tilde{\lambda}_i \tilde{F}^\dagger \tilde{X}_L d_R^i + h.c. \quad (18)$$

Fig.8 shows the required value of $\tilde{\lambda}_b$ for the correct relic abundance of DM within 1σ . As mentioned above, the s -wave contribution is efficient to reduce the abundance and then $\tilde{\lambda}_b$ is relatively small in the parameter region. This leads the small cross section for the direct detection of \tilde{X} , so that even XENON-1T could cover only the compressed region. The blue region is excluded by the $bb + E_T^{\text{miss}}$ at the LHC, where the production cross section of the extra scalars at the LO exceeds the experimental upper bounds using the same data as the case of extra fermions. Note that the parameter region of Fig. 8 seems to face the stringent constraint from the latest AMS-02 result [27, 28].

We also estimate the triviality bound. The beta functions for $\tilde{\lambda}_b$ and the QCD coupling are given as follows.

$$\beta_{\tilde{\lambda}_b} \simeq \frac{1}{(4\pi)^2} \left(-4g_3^2 + 3\tilde{\lambda}_b^2 \right) \tilde{\lambda}_b, \quad (19)$$

$$\beta_{g_3} \simeq \frac{1}{(4\pi)^2} \left(-\frac{41}{6}g_3^3 \right). \quad (20)$$

We fill the region where the triviality bound is below 10^{18} GeV and 1000 TeV with green color in Fig. 8. The bound is weaker than in the scalar DM case because the required Yukawa coupling to reproduce the correct relic abundance is smaller than in the scalar DM case.

5 Summary

DM is one of promising particles which will be discovered near future. There are a lot of possibilities of DM models, and we seriously have to examine what kind of DM models can explain the DM abundance in our universe without any conflict with the other experimental results. In the Weakly Interacting Massive Particle scenario, we may be able to classify DM models, in terms of interactions between DMs and quarks/leptons. If DMs interact with the SM particles via the electroweak gauge couplings, the gauge interactions would be dominant and effective to achieve the relic abundance of DMs. If DMs are SM gauge singlets, new interactions would be required as far as the Higgs exchanging is not so efficient. In this paper, we focus on one possibility that two DMs annihilate into two quarks in the t -channel given by extra-quark exchanging. Interestingly, the new interaction is flavor-dependent, so that this simple DM model can be tested by flavor physics as well as DM physics and the LHC experiments. If DM signals are confirmed in the direct/indirect detections of DMs or/and the LHC experiments, we have to find out a promising DM model among many candidates, using independent physical observables. In our model, we can expect that some correlations and explicit predictions exist in observables of flavor physics, so that we are sure that our simple model can be tested by the accurate measurements of the flavor violating processes. In fact, our region to explain the relic DM abundance is very close to the exclusion limit of the DM direct detections in the scalar DM case, so that our DM may be discovered near future. Besides, the Belle II experiment will start in 2018 and the measurements of the new physics contributions to flavor physics, e.g. the $\Delta F = 2$ processes, expected to be drastically improved [30]. Then, our models can be tested via the observations of the $\Delta F = 2$ processes with the great accuracies. Our setup is very simple and predicts distinguishing deviations from the SM predictions in flavor physics. Moreover, the thermal relic abundance of the DM suggests the large Yukawa coupling of the DM with bottom quark, so that the deviations in the $\Delta F = 2$ processes are sizable. Interestingly, a discrepancy of the observables in the $\Delta F = 2$ processes has been proposed in Ref. [39]. It will be important to discuss the consistency with the observations, considering the discrepancy [40].

In order to compare with another DM model, we also present our results in Dirac-fermion DM case. There are still a lot of possible setups which are not studied here: real scalar DM case, *top partner* model and so on. It is very important to clearly understand the differences among them and to prepare for the discovery of DMs. We have to find out how to test and distinguish DM models. The study for the comparison is ongoing. Note that our model presented here is one of the realist setups to evade the stringent bound from the indirect detection of DM [27, 28].

Acknowledgments

We are grateful to C. Boehm, A. J. Buras and A. Ibarra for comments and suggestions. This work was supported by JSPS KAKENHI Grant Number 16K17715 [TA]. The work of J. K. was supported by Grant-in-Aid for Research Fellow of Japan Society for the Promotion of Science No. 16J04215.

A Functions

The functions which appear in $K_0\text{--}\bar{K}_0$ mixing are given by

$$S_0(x) = \frac{4x - 11x^2 + x^3}{4(1-x)^2} - \frac{3x^3 \log x}{2(1-x)^3}, \quad (21)$$

$$S(x, y) = \frac{-3xy}{4(y-1)(x-1)} - \frac{xy(4-8y+y^2) \log y}{4(y-1)^2(x-y)} + \frac{xy(4-8x+x^2) \log x}{4(x-1)^2(x-y)}. \quad (22)$$

References

- [1] G. Hinshaw *et al.* [WMAP Collaboration], *Astrophys. J. Suppl.* **208**:19 (2013) [arXiv:1212.5226 [astro-ph.CO]].
- [2] P. A. R. Ade *et al.* [Planck Collaboration], *Astron. Astrophys.* **594**, A13 (2016) [arXiv:1502.01589 [astro-ph.CO]].
- [3] M. Cirelli, N. Fornengo and A. Strumia, *Nucl. Phys. B* **753**, 178 (2006) [hep-ph/0512090].
- [4] P. Fileviez Perez and M. B. Wise, *JHEP* **1305**, 094 (2013) [arXiv:1303.1452 [hep-ph]].
- [5] S. Chang, R. Edezhath, J. Hutchinson and M. Luty, *Phys. Rev. D* **89**, no. 1, 015011 (2014) [arXiv:1307.8120 [hep-ph]].
- [6] Y. Bai and J. Berger, *JHEP* **1311**, 171 (2013) [arXiv:1308.0612 [hep-ph]].
- [7] C. Kilic, M. D. Klimek and J. H. Yu, *Phys. Rev. D* **91**, no. 5, 054036 (2015) [arXiv:1501.02202 [hep-ph]].
- [8] F. Giacchino, A. Ibarra, L. Lopez Honorez, M. H. G. Tytgat and S. Wild, *JCAP* **1602**, no. 02, 002 (2016) [arXiv:1511.04452 [hep-ph]].
- [9] J. Kawamura and Y. Omura, *Phys. Rev. D* **93**, no. 11, 115011 (2016) [arXiv:1601.07396 [hep-ph]].

- [10] S. Baek, P. Ko and P. Wu, JHEP **1610**, 117 (2016) [arXiv:1606.00072 [hep-ph]].
- [11] P. Agrawal, S. Blanchet, Z. Chacko and C. Kilic, Phys. Rev. D **86**, 055002 (2012) [arXiv:1109.3516 [hep-ph]].
- [12] P. Agrawal, M. Blanke and K. Gemmler, JHEP **1410**, 72 (2014) [arXiv:1405.6709 [hep-ph]].
- [13] B. Bhattacharya, D. London, J. M. Cline, A. Datta and G. Dupuis, Phys. Rev. D **92**, no. 11, 115012 (2015) [arXiv:1509.04271 [hep-ph]].
- [14] C. Degrande, C. Duhr, B. Fuks, D. Grellscheid, O. Mattelaer and T. Reiter, Comput. Phys. Commun. **183**, 1201 (2012) [arXiv:1108.2040 [hep-ph]].
- [15] A. Alloul, N. D. Christensen, C. Degrande, C. Duhr and B. Fuks, Comput. Phys. Commun. **185**, 2250 (2014) [arXiv:1310.1921 [hep-ph]].
- [16] J. Alwall, R. Frederix, S. Frixione, V. Hirschi, F. Maltoni, O. Mattelaer, H.-S. Shao and T. Stelzer *et al.*, JHEP **1407**, 079 (2014) [arXiv:1405.0301 [hep-ph]].
- [17] T. Sjostrand, S. Mrenna and P. Z. Skands, JHEP **0605**, 026 (2006) [hep-ph/0603175].
- [18] J. de Favereau *et al.* [DELPHES 3 Collaboration], JHEP **1402**, 057 (2014) [arXiv:1307.6346 [hep-ex]].
- [19] F. Caravaglios, M. L. Mangano, M. Moretti and R. Pittau, Nucl. Phys. B **539**, 215 (1999) [hep-ph/9807570].
- [20] M. Cacciari, G. P. Salam and G. Soyez, JHEP **0804**, 063 (2008) [arXiv:0802.1189 [hep-ph]].
- [21] The ATLAS collaboration, ATLAS-CONF-2015-066.
- [22] G. Belanger, F. Boudjema, A. Pukhov and A. Semenov, Comput. Phys. Commun. **185**, 960 (2014) [arXiv:1305.0237 [hep-ph]].
- [23] M. Ackermann *et al.* [Fermi-LAT Collaboration], Phys. Rev. Lett. **115**, no. 23, 231301 (2015) [arXiv:1503.02641 [astro-ph.HE]].
- [24] D. S. Akerib *et al.* [LUX Collaboration], Phys. Rev. Lett. **116**, no. 16, 161301 (2016) [arXiv:1512.03506 [astro-ph.CO]].
- [25] D. S. Akerib *et al.*, arXiv:1608.07648 [astro-ph.CO].
- [26] A. Tan *et al.* [PandaX-II Collaboration], Phys. Rev. Lett. **117**, no. 12, 121303 (2016) [arXiv:1607.07400 [hep-ex]].
- [27] A. Cuoco, M. Krämer and M. Korsmeier, arXiv:1610.03071 [astro-ph.HE].

- [28] M. Y. Cui, Q. Yuan, Y. L. S. Tsai and Y. Z. Fan, arXiv:1610.03840 [astro-ph.HE].
- [29] M. Aguilar et al. (AMS), Phys. Rev. Lett. **117**, 091103 (2016).
- [30] J. Charles, S. Descotes-Genon, Z. Ligeti, S. Monteil, M. Papucci and K. Trabelsi, Phys. Rev. D **89**, no. 3, 033016 (2014) [arXiv:1309.2293 [hep-ph]].
- [31] K. A. Olive *et al.* [Particle Data Group], Chin. Phys. C **38** (2014) 090001.
- [32] Jack Laiho, E. Lunghi and Ruth S. Van de Water, Phys. Rev. D **81** (2010) 034503 [arXiv:0910.2928 [hep-ph]].
See also the latest values in <http://www.latticeaverages.org>.
- [33] J. Brod and M. Gorbahn, Phys. Rev. Lett. **108**, 121801 (2012) [arXiv:1108.2036 [hep-ph]].
- [34] A. J. Buras, M. Jamin and P. H. Weisz, Nucl. Phys. B **347**, 491 (1990).
- [35] J. Brod and M. Gorbahn, Phys. Rev. D **82**, 094026 (2010) [arXiv:1007.0684 [hep-ph]].
- [36] J. Charles *et al.*, Phys. Rev. D **91**, no. 7, 073007 (2015) [arXiv:1501.05013 [hep-ph]].
- [37] S. Descotes-Genon, J. Matias and J. Virto, Phys. Rev. D **88**, 074002 (2013) [arXiv:1307.5683 [hep-ph]].
- [38] G. Hiller and M. Schmaltz, Phys. Rev. D **90**, 054014 (2014) [arXiv:1408.1627 [hep-ph]].
- [39] M. Blanke and A. J. Buras, Eur. Phys. J. C **76**, no. 4, 197 (2016) [arXiv:1602.04020 [hep-ph]].
- [40] Work in progress.